AGU ADVANCING EARTH AND SPACE SCIENCES

AGU Advances

RESEARCH ARTICLE
10.1029/2025AV001865

Anthropogenically Stimulated Carbonate Dissolution in the Global Shelf Seafloor Is Potentially an Important and Fast Climate Feedback

Sebastiaan J. van de Velde[1,2,3], **Pam Vervoort**[4], **Robert O. Smith**[1], **Cliff S. Law**[1,2], **and Kim Currie**[2]

[1]Department of Marine Science, University of Otago, Dunedin, New Zealand, [2]Earth Sciences New Zealand, Wellington, New Zealand, [3]Department of Biology, University of Antwerp, Wilrijk, Belgium, [4]School of Geography, Earth, and Environmental Sciences, University of Birmingham, Birmingham, UK

Peer Review The peer review history for this article is available as a PDF in the Supporting Information.

Key Points:

- Ocean acidification has been increasing calcium carbonate dissolution in the east Otago shelf seafloor over the past 25 years
- Increased carbonate dissolution potentially represents a fast climate feedback that operates on annual-decadal timescales
- The inclusion of the fast carbonate dissolution feedback in models could partially close the current model-data gap in ocean carbon budgets

Supporting Information:

Supporting Information may be found in the online version of this article.

Correspondence to:

S. J. van de Velde,
sebastiaan.vandevelde@otago.ac.nz

Citation:

van de Velde, S. J., Vervoort, P., Smith, R. O., Law, C. S., & Currie, K. (2026). Anthropogenically stimulated carbonate dissolution in the global shelf seafloor is potentially an important and fast climate feedback. *AGU Advances*, *7*, e2025AV001865. https://doi.org/10.1029/2025AV001865

Received 21 MAY 2025
Accepted 31 OCT 2025

Author Contributions:

Conceptualization: Sebastiaan J. van de Velde
Data curation: Sebastiaan J. van de Velde, Kim Currie
Formal analysis: Sebastiaan J. van de Velde, Pam Vervoort
Funding acquisition: Cliff S. Law, Kim Currie
Investigation: Sebastiaan J. van de Velde, Pam Vervoort, Robert O. Smith, Kim Currie

Abstract Carbonate mineral production and dissolution regulate atmospheric carbon dioxide (CO_2) concentrations via modulation of the ocean alkalinity content. The anthropogenic rise in atmospheric CO_2 reduces calcification rates and enhances calcium carbonate dissolution, which increases ocean alkalinity, counteracts acidification, and stimulates ocean CO_2 uptake. However, carbonate dissolution takes place primarily in the deep ocean, so this feedback is slow, maintaining ocean CO_2 uptake over millennial timescales. Here, we present evidence that seawater alkalinity on the continental shelf is increasing on annual-decadal timescales, at a rate that is orders of magnitude faster than the deep ocean feedback. Biogeochemical model analyses suggest this fast feedback results from calcium carbonate dissolution in the shelf seafloor driven by increasing atmospheric CO_2 concentrations. Extrapolating these results to the global continental shelf suggests that shelf carbonate dissolution has been accelerating since the 1800s and may account for up to 10% of the missing ~0.3 Pg C yr^{-1} in ocean model carbon budgets.

Plain Language Summary The natural calcium carbonate buffer of the ocean helps to keep the atmospheric carbon dioxide concentrations in check. As atmospheric carbon dioxide levels increase, the ocean becomes more acidic, which stimulates the dissolution of calcium carbonate minerals, removes atmospheric carbon dioxide, and decreases ocean acidity again. This calcium carbonate buffer feedback is assumed to mainly take place in the deep ocean below 500 m and was a slow process, taking >1,000 years to respond to changes in atmospheric carbon dioxide concentrations. Here, we use a 25-year monitoring data set to show that this calcium carbonate buffer has been active in shallow waters (less than 200 m depth) offshore Aotearoa New Zealand for at least the past 25 years. The shallow calcium carbonate buffer responds on annual-decadal timescales and thus represents a fast natural climate feedback that is not considered in global carbon models.

1. Introduction

The Earth's climate is stabilized by negative feedback loops between atmospheric carbon dioxide (CO_2) concentrations and the supply of alkalinity (A_T, or total alkalinity) to the ocean (Friedlingstein et al., 2025; Hönisch et al., 2012; Zeebe & Wolf-Gladrow, 2001). Higher ocean A_T, which is the excess of proton acceptors (bases) over proton donors (acids), allows more CO_2 to be stored in the ocean in the form of dissolved inorganic carbon (DIC) (Zeebe & Wolf-Gladrow, 2001). The primary processes modulating ocean A_T are supply from terrestrial weathering via rivers and the balance between calcium carbonate ($CaCO_3$) precipitation in the surface ocean and dissolution in the deep ocean, which determines the eventual $CaCO_3$ burial in the seafloor (Boudreau et al., 2010; Zeebe, 2012). Terrestrial weathering is the slowest of these feedback loops, operating over >10,000-year timescales (Archer, 2005). As atmospheric CO_2 increases, higher temperatures and increased rainfall stimulate the dissolution of silicate and carbonate rocks on land, leading to higher A_T production and increase atmospheric CO_2 uptake by the ocean (Archer, 2005; Berner, 1991).

The deep-sea $CaCO_3$ dissolution feedback is driven by a decrease in the $CaCO_3$ saturation state (Ω) of seawater with respect to minerals such as aragonite ($\Omega_{aragonite}$) and calcite ($\Omega_{calcite}$) in response to rising CO_2 concentrations in the ocean. Calcifying organisms form $CaCO_3$ in the surface ocean, which consumes two moles of A_T per mole of $CaCO_3$ formed. As most surface ocean waters are oversaturated with respect to $CaCO_3$ ($\Omega > 1$), these particles do not dissolve efficiently, allowing them to settle through the ocean. Microbial respiration of organic matter

Methodology: Sebastiaan J. van de Velde, Pam Vervoort, Kim Currie
Project administration: Sebastiaan J. van de Velde, Cliff S. Law, Kim Currie
Software: Sebastiaan J. van de Velde, Pam Vervoort
Validation: Sebastiaan J. van de Velde
Visualization: Sebastiaan J. van de Velde
Writing – original draft: Sebastiaan J. van de Velde
Writing – review & editing: Sebastiaan J. van de Velde, Pam Vervoort, Robert O. Smith, Cliff S. Law, Kim Currie

(OM) decreases the saturation state in the deeper ocean layers until the $CaCO_3$ saturation horizon is reached, the depth below which water becomes undersaturated ($\Omega < 1$) and where $CaCO_3$ dissolution is thermodynamically favorable (Boudreau et al., 2010; Zeebe, 2012). Above this horizon, $CaCO_3$ accumulates efficiently in the seafloor, whereas below this depth, $CaCO_3$ minerals dissolve in both the water column and seafloor. This process is called the "carbonate pump" which removes A_T from the surface ocean and thereby reduces the CO_2 uptake capacity of the surface ocean (Volk & Hoffert, 1985). When atmospheric CO_2 concentrations increase, the Ω of the ocean decreases, which results in reduced $CaCO_3$ precipitation, and an upward migration of the $CaCO_3$ saturation horizon to shallower depths (Boudreau et al., 2010; Zeebe, 2012). The shoaling of the $CaCO_3$ saturation horizon exposes a larger fraction of the deep seafloor to undersaturated conditions, and so the resulting additional $CaCO_3$ dissolution increases ocean A_T. As the $CaCO_3$ saturation horizon generally lies at water depths below 500 m, higher A_T waters only resurface after >1,000 years (Cao et al., 2009), and so this feedback is too slow to compensate for anthropogenic emissions on human-relevant timescales (Boudreau et al., 2010).

In contrast, continental shelf sediments are located at shallower water depths (<200 m), where the overlying water column can become vertically well mixed on sub-seasonal to annual timescales and the mixed later can reach the seafloor (Johnson et al., 2023; D. C. Jones et al., 2014). As a result, there is a strong connection between the seafloor and lower atmosphere, which suggests that seafloor processes can potentially influence atmospheric CO_2 on human-relevant timescales. $CaCO_3$ dissolution in the shallow seafloor occurs when seafloor remineralization rates are sufficiently large to cause porewater undersaturation (Aller, 1982; Kessler et al., 2020; Morse & Mackenzie, 1990). Studies in carbonate reef sands (~4% of the continental shelf) have shown an increase in seafloor carbonate dissolution with decreasing Ω in the overlying water (Albright et al., 2016; Eyre et al., 2018; Kessler et al., 2020). However, carbonate-poor sands, which represent the majority (>60%) of the global continental shelf are generally assumed to undergo negligible $CaCO_3$ dissolution (Andersson et al., 2003, 2006; Morse et al., 2006). Yet, A_T production from $CaCO_3$ dissolution in carbonate-poor sandy sediments of California increased within hours to a decrease in the Ω of the overlying water (Lunstrum & Berelson, 2022). This raises the intriguing possibility of a "fast climate feedback," if $CaCO_3$ dissolution in the continental shelf seafloor can remove significant atmospheric CO_2.

Currently, state-of-the-art global ocean models project a marine CO_2 sink that is ~0.3 Pg C yr^{-1} (10% of the global ocean sink) lower than available data products suggest, and this discrepancy has seemingly been increasing over time (Friedlingstein et al., 2025). This model-data mismatch alludes to a missing carbon cycle process in models, and enhanced $CaCO_3$ dissolution in the shelf seafloor could account for both the model-data anomaly and the increasing anomaly with time. To investigate this possibility, we analyzed trends in shelf water $\Omega_{aragonite}$ and A_T in a 25-year long time series from shelf waters of south-east Aotearoa New Zealand (Figure 1). We then developed a model of the drivers of the observed A_T increase and implemented the results in an Earth system model of intermediate complexity (EMIC) to investigate whether the fast feedback could close the gap between model and data estimates of global ocean CO_2 uptake.

2. Materials and Methods

2.1. Munida Carbonate Chemistry Monitoring Time Series

The Munida time series is the longest-running time series of ocean carbonate chemistry observations in the southern hemisphere, located offshore Ōtepoti Dunedin on the southeast coast of Te Waipounamu (South Island) of Aotearoa New Zealand (Currie, Reid, et al., 2011; Vance et al., 2024) (Figure 1). The full transect consists of nine stations from low-salinity shelf/neritic waters nearest the coast, crossing saltier modified subtropical water, the subtropical front, into low-salinity subantarctic waters. The unique aspect of the Munida time series is that it is the only global time series that has collected high-precision A_T measurements in continental shelf waters over decadal timescales, so enabling discrimination of the low-level temporal trends from the high interannual variability. Here, we compare data for the shelf station (170.8083°E, 45.7771°S) and the subantarctic station (171.5369°E, 45.83004°S), with use of these two end member stations avoiding variability associated with the dynamic subtropical front. The mixed-layer depth over the mid to outer continental shelf fluctuates between 10m and the full water column depth over seasonal and weather-band timescales (Johnson et al., 2023; K. N. Jones et al., 2013), with no significant temporal trend over the period of 1998–2021 (Figure S1 in Supporting Information S1). The shelf seafloor consists of a mixture of sand and mud, and is characterized by a porosity of ~0.5, low organic carbon contents (<1.0 wt.% C), and low $CaCO_3$ contents (<0.8 wt.% C).

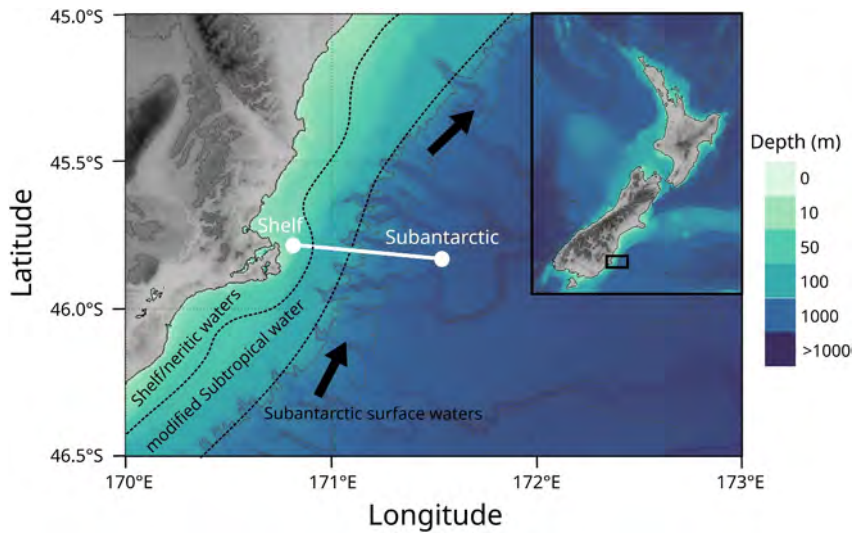

Figure 1. Stations and data from the "Munida" time series. Field site with indication of the Munida transect line and the shelf and subantarctic stations. Indicated are the approximate boundaries between the shelf/neritic, subtropical and subantarctic water masses together with their general northeastward circulation (Chiswell et al., 2015; Hopkins et al., 2010; K. N. Jones et al., 2013).

Alkalinity (A_T) was measured following standard operating procedures (SOP) using an automated potentiometric closed cell titration (Dickson et al., 2007). The titration data was analyzed by a least squares optimization technique. The accuracy was estimated to be within 1.0 μmol kg^{-1}, and precision is estimated to be <4.0 μmol kg^{-1} based on the repeated analysis of duplicate samples and reference materials (Currie, Macaskill, et al., 2011). Alkalinity (A_T) of Clutha river water was measured following SOP using an automated potentiometric open cell titration (Dickson et al., 2007), with similar accuracy and precision. Surface water partial pressure of CO_2 (pCO_2) was measured continuously using an equilibration system with infrared analysis as detailed in (Currie, Reid, et al., 2011). $\Omega_{aragonite}$ was calculated from measured A_T, pCO_2, temperature, and salinity using CRAN:seacarb (Gattuso et al., 2024). Alkalinity time series were analyzed following the current best practices of ocean acidification time series (A. J. Sutton et al., 2022). Results of the time series analysis are reported as slope ± standard error.

2.2. Otago Coast Box Model

To test our hypothesis that changes in pelagic calcification and benthic $CacO_3$ dissolution drive an alkalinity increase in the east Otago shelf waters, we developed a model of A_T and $CaCO_3$ cycling on the east Otago shelf. The model domain ranged from the mouth of the Clutha in the south to Shag point in the north, and from the coastline in the west to the edge of the shelf in the east (Figure 2a), which is the same domain used in previous

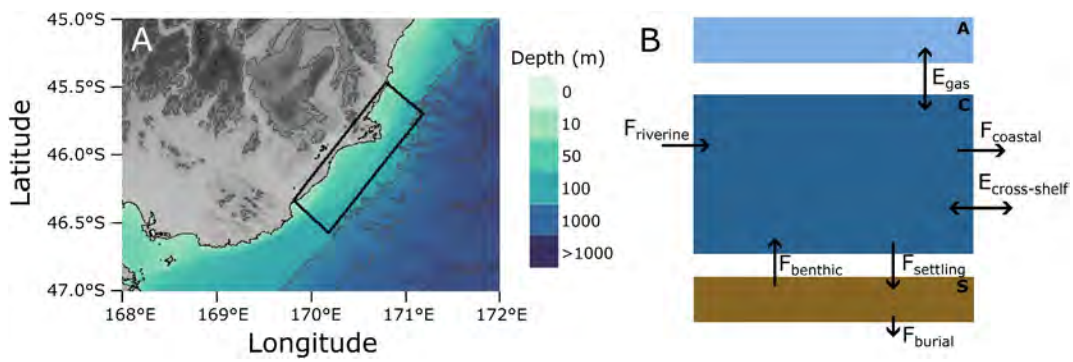

Figure 2. East Otago shelf box model. (a) Model domain indicated by the black box. (b) Conceptual model description of the three boxes representing the atmosphere (A), the shelf waters (C), and the shelf seafloor (S). See main text for details.

studies of the east Otago shelf and captures the key features of the $CaCO_3$ budget for this part of Aotearoa (Carter, 1986; Johnson et al., 2024). The Otago shelf waters undergo frequent full water column vertical mixing, both on time scales of monthly or faster (Johnson et al., 2023, 2024), which enables approximation of the whole shelf using three boxes (Figure 2b); one representing the shelf waters (C), one representing the atmosphere (A), and one the shelf seafloor (S). The model included four state variables: alkalinity in the shelf waters ($A_{T,C}$), DIC in the shelf waters (DIC_C), calcium carbonate in the shelf waters ($CaCO_{3,C}$), and calcium carbonate in the seafloor ($CaCO_{3,S}$). We did not explicitly model aragonite or calcite, but simulated a total pool of $CaCO_3$, including all polymorphs. For the pelagic model, this grouping has no impact, as calcification affects A_T the same for all polymorphs. For the benthic model, we assumed that half of the $CaCO_3$ pool consisted of aragonite, which is the fastest dissolving $CaCO_3$ mineral and controls the bulk benthic dissolution rate of $CaCO_3$ (Sulpis, Agrawal, et al., 2022). Gaseous CO_2 is exchanged between atmosphere and shelf waters (E_{gas}), particulate $CaCO_3$ settles to the seafloor ($F_{settling}$), while A_T and DIC produced during $CaCO_3$ dissolution are returned to the shelf waters as a benthic flux ($F_{benthic}$). Part of the $CaCO_3$ that is not dissolved is eventually buried (F_{burial}). $CaCO_3$, A_T, and DIC come into the shelf box via riverine input ($F_{riverine}$) from the Clutha and Taieri, the main rivers on the east Otago coast (Carter, 1986; Johnson et al., 2024). $CaCO_3$, A_T, and DIC are transferred along the coastal current ($F_{coastal}$), and part of the shelf waters are mixed with the offshore subtropical waters in cross-shelf exchange ($E_{cross\text{-}shelf}$).

2.2.1. Pelagic Model

Gas exchange between the atmosphere (A) and shelf waters (C) is parameterized using a fixed transfer velocity following standard modeling practices (Raymond & Cole, 2001; Ridgwell, Hargreaves, et al., 2007; van de Velde, Reinhard, et al., 2020). We used a high piston velocity ($k_{transfer}$), which assumes instant equilibration between atmosphere and ocean—an appropriate approximation on decadal timescales.

$$E_{gas} = k_{transfer} A_C \left([CO_2]_{eq} - [CO_2]_C\right) \quad (1)$$

where A_C is the surface area of the shelf box. The equilibrium CO_2 concentration $[CO_2]_{eq}$ was calculated from the atmospheric pCO_2, alkalinity of the shelf box ($A_{T,C}$), salinity, and temperature using the CRAN:seacarb package (Gattuso et al., 2024) and the dissociation constants for carbonic acid from Lueker et al. (2000). Since there was no discernible change in riverine discharge of either the Clutha River or the Taieri river, riverine input was calculated using the mean discharge of the river over the past 24 years (available from Otago Regional Council and NIWA)

$$F_{riverine} = Q_{river} X_{river} \quad (2)$$

where X is $[CaCO_3]$, A_T, or [DIC]. Cross-shelf exchange was implemented by exchanging water between the shelf box and the open ocean, which was calculated using the water flux between the shelf waters and offshore waters (which was derived from the shelf residence time, see below)

$$E_{cross\text{-}shelf} = Q_{cross\text{-}shelf} \left(X_C - X_{ocean}\right) \quad (3)$$

where X is $[CaCO_3]$, A_T, or [DIC]. Settling of $CaCO_3$ was calculated using a fixed settling velocity ($v_{settling}$)

$$F_{settling} = v_{settling} A_{seafloor} [CaCO_3]_C \quad (4)$$

where $A_{seafloor}$ is the surface area of the seafloor box. Analogously, burial of $CaCO_3$ was calculated a fixed burial velocity (v_{burial})

$$F_{burial} = v_{burial} A_{seafloor} [CaCO_3]_S \quad (5)$$

The reaction set was chosen to represent a parsimonious description of $CaCO_3$ and A_T cycling in the Otago shelf, and so we only consider calcification in box C ($R_{calcification}$). Calcification produces one mol of $CaCO_3$ and consumes two mol of A_T and one mol of DIC, $CaCO_3$ dissolution in the seafloor consumes one mol of $CaCO_3$ and produces two mol of A_T and one mol of DIC.

The resulting set of mass balance equations then becomes

$$\begin{cases} \dfrac{\partial A_{TC}}{\partial t} = Q_{\text{Clutha}}A_{T\text{Clutha}} + Q_{\text{Taieri}}A_{T\text{Taieri}} - Q_{\text{cross-shelf}}\left(A_{TC} - A_{T\text{ocean}}\right) - Q_{\text{coastal}}A_{TC} \\ \qquad + F_{\text{benthic},A_T}A_{\text{seafloor}} - 2R_{\text{calcification}} \\ \dfrac{\partial [\text{DIC}]_C}{\partial t} = Q_{\text{Clutha}}[\text{DIC}]_{\text{Clutha}} + Q_{\text{Taieri}}[\text{DIC}]_{\text{Taieri}} - Q_{\text{cross-shelf}}\left([\text{DIC}]_C - [\text{DIC}]_{\text{ocean}}\right) - Q_{\text{coastal}}[\text{DIC}]_C \\ \qquad + F_{\text{benthic,DIC}}A_{\text{seafloor}} - R_{\text{calcification}} + k_{\text{transfer}}A_C\left([\text{CO}_2]_{\text{eq}} - [\text{CO}_2]_C\right) \\ \dfrac{\partial [\text{CaCO}_3]_C}{\partial t} = Q_{\text{Clutha}}[\text{CaCO}_3]_{\text{Clutha}} + Q_{\text{Taieri}}[\text{CaCO}_3]_{\text{Taieri}} - Q_{\text{cross-shelf}}\left([\text{CaCO}_3]_C - [\text{CaCO}_3]_{\text{ocean}}\right) \\ \qquad - Q_{\text{coastal}}[\text{CaCO}_3]_C - v_{\text{settling}}A_{\text{seafloor}}[\text{CaCO}_3]_C + R_{\text{calcification}} \\ \dfrac{\partial [\text{CaCO}_3]_S}{\partial t} = v_{\text{settling}}A_{\text{seafloor}}[\text{CaCO}_3]_C - v_{\text{burial}}A_{\text{seafloor}}[\text{CaCO}_3]_S - R_{\text{dissolution}} \end{cases}$$

Calcification in the water column is dependent on the calcite saturation state (Ω_{calcite}) using a linear best fit derived from a compilation of different calcifying algae and corals (Gattuso et al., 1999), consistent with the approach followed by previous modeling studies (Andersson et al., 2003, 2006)

$$R_{\text{calcification}} = \frac{(21.3\Omega_{\text{calcite}} + 12)}{(21.3\Omega_{\text{calcite,ref}} + 12)}R_{\text{calcification,ref}} \tag{6}$$

where the reference rate of calcification ($R_{\text{calcification,ref}}$) was constrained using available data from the east Otago shelf, and the reference saturation state $\Omega_{\text{calcite,ref}}$ was the saturation state in the year 1998. Following (Andersson et al., 2003), we tested an alternative formulation based on a curvilinear relationship of *Stylophora pistillata* (Gattuso et al., 1998; Leclercq et al., 2002)

$$R_{\text{calcification}} = 228\,\frac{\left(1 - e^{\Omega_{\text{calcite}}/0.69}\right)}{\left(1 - e^{\Omega_{\text{calcite,ref}}/0.69}\right)}R_{\text{calcification,ref}} \tag{7}$$

which produced a poorer model-data fit (Figure S2 in Supporting Information S1) and is not surprising given that this relationship is based on a single species of tropical coral reef that is not present on the east Otago shelf. Nevertheless, overall model behavior was identical. $CaCO_3$ dissolution in the seafloor was implemented by integrating a one-dimensional seafloor model (see below) into the box-model using a meta-modeling approach (Soetaert et al., 2000). Model parameters are summarized in Table 1.

2.2.2. Shelf Seafloor Model

The seafloor model (S) was designed to represent $CaCO_3$ dissolution in a sandy sediment column that is dominated by advective porewater flow. The model has a classical structure of an early diagenetic model (Boudreau, 1997; Soetaert et al., 1996). Because of the advective flow and well-mixed nature of sandy continental shelf sediments, we ignored any transport induced by benthic fauna, which means the mass balance equations become

$$\varphi\frac{\partial C_i}{\partial t} = \frac{\partial}{\partial z}\left(\varphi D_i\frac{\partial C_i}{\partial z} - \varphi v C_i\right) + \sum_k \upsilon_{i,k}R_k \tag{8}$$

where C_i is the concentration of a solute in the porewater, D_i is the effective diffusion coefficient (calculated as $D_i = \frac{D_0(S,T)}{1 - 2\ ln\ \varphi}$; Boudreau, 1996), φ is the porosity, v is the advective porewater flow, and $\upsilon_{i,k}$ denotes the stoichiometric coefficient of the ith species in the kth reaction. For each solute, D_0 was derived from salinity and temperature using the "diffcoeff" function in the CRAN:marelac package (Soetaert et al., 2010).

Table 1
Parameters Used in the East Otago Coast Box Model

Parameter	Symbol	Value	Unit	Source
Water height	h_{water}	30	m	Mitchell et al. (2012)
Surface area	A	4,125	km^2	
Seafloor height	$h_{seafloor}$	5	cm	Huettel et al. (1998, 2014), Precht et al. (2004)
Settling velocity	$v_{settling}$	0–10	cm s^{-1}	McCandliss et al. (2002)
Burial velocity	v_{burial}	0–0.025	cm yr^{-1}	Carter (1986)
Gas transfer velocity	$k_{transfer}$	5.0	m d^{-1}	Raymond and Cole (2001)
Shelf water residence time	RT_{shelf}	10–90	d	Johnson et al. (2024), Liu et al. (2019)
Discharge Clutha river	Q_{Clutha}	574	m^3 s^{-1}	Otago Regional Council (2025)
Discharge Taieri River	Q_{Taieri}	36	m^3 s^{-1}	Otago Regional Council (2025)
Salinity	S	34.5	–	Munida data
Temperature	T	12.0	°C	Munida data
Dry sediment density	ρ_{sed}	2.6	g cm^{-3}	
Porosity	Φ	0.4	–	
Alkalinity open ocean	$A_{T,ocean}$	2,300	µmol kg^{-1}	Munida data
Alkalinity Clutha	$A_{T,Clutha}$	0.0–1,500	µmol kg^{-1}	Kim et al. (1996)
Alkalinity Taieri	$A_{T,Taieri}$	0.0–1,250	µmol kg^{-1}	Kim and Hunter (2001)
$CaCO_3$ Clutha	$[CaCO_3]_{Clutha}$	0.0028–0.0044	µmol cm^{-3}	Carter (1986), G. Müller et al. (2022)
$CaCO_3$ Taieri	$[CaCO_3]_{Taieri}$	0.049–0.078	µmol cm^{-3}	Carter (1986), G. Müller et al. (2022)
Calcification rate	R_{CaCO_3}	0–2,650	µmol cm^{-3} yr^{-1}	Carter (1986), A. M. Smith et al. (2010)
Atmospheric CO_2 concentration	pCO_2	Variable	ppm	Meinshausen et al. (2017, 2020)

Note. Single values are fixed parameters, values given as a range are parameters included in the Monte Carlo sensitivity simulations (see main text).

The model design was tailored to the short-term experiments of Lunstrum and Berelson (2022), and therefore included only dissolved species as state variables; dissolved oxygen (O_2), DIC, A_T, nitrate (NO_3^-), ammonium (NH_4^+), and dissolved sulfide (H_2S). Lunstrum and Berelson (2022) only measured O_2, DIC, and A_T, but we included the other species to account for A_T loss during ammonium oxidation, as well as A_T production during anaerobic mineralization (Hu & Cai, 2011; Middelburg et al., 2020). The reaction set contains eight reactions; OM mineralization coupled to aerobic respiration (AR), denitrification (DN), and sulfate reduction (SR), the sequential usage of which were implemented via conventional limitation-inhibition formulations (Table 2) (Soetaert et al., 1996). Reduced ammonium and sulfide can be oxidized by O_2 during nitrification (NIT) and sulfide oxidation (SOx) respectively. Finally, the model included calcite dissolution (CaD), aragonite dissolution (ArD), and calcite precipitation (CaP). The set of carbonate mineral dissolution-precipitation reactions was implemented using the new formulations that allow for a continuum between $CaCO_3$ dissolution and precipitation (Sulpis, Humphreys, et al., 2022). We did not explicitly model OM and sulfate, as we assumed that mineralization is not limited by OM availability and that SR is not limited by sulfate availability.

The numerical model solution was implemented following the procedures outlined in Soetaert and Meysman (2012) in the open-source programming language R (R Core Team, 2021). A sediment grid was generated by dividing the sediment domain into 100 layers of identical thickness, over which the spatial derivatives were expanded using finite differences using CRAN:ReacTran (Soetaert & Meysman, 2012). The resulting set of ordinary differential equations was then solved for steady state using the solver 'stode' within the package CRAN: rootSolve (Soetaert, 2009). Model parameters and boundary conditions are summarized in Tables 3 and 4.

The shelf seafloor model was validated by repeating the experiments described in Lunstrum and Berelson (2022). Briefly, a sediment column of varying length (8.5, 18.5, 26 cm) and different flow rates (0.5, 1, 2 cm^3 min^{-1}) was simulated. This yielded porewater residence times of 1.8, 3.6, and 5.4 hr. The A_T of the inflowing water was adjusted at a constant pCO_2, to reach $\Omega_{aragonite}$ of 1.04, 1.29, 2.42, and 2.43 (Table 3). Subsequently, we compared the total amount of $CaCO_3$ that was dissolved over the course of the experiment (Figure 3a), and the total A_T

Table 2
Reaction Set From the Sediment Model

Reaction	Stoichiometric equation	Kinetic rate expression
Aerobic respiration (AR)	$OM + O_2 \rightarrow CO_2 + \frac{16}{106}NH_4^+ + \frac{15}{106}OH^-$	$R_{\min}\frac{[O_2]}{K_{O_2}+[O_2]}$
Denitrification (DN)	$OM + \frac{4}{5}NO_3^- \rightarrow CO_2 + \frac{2}{5}N_2 + \frac{99.8}{106}OH^-$	$R_{\min}\frac{[NO_3^-]}{K_{NO_3^-}+[NO_3^-]}\frac{K_{O_2}}{K_{O_2}+[O_2]}$
Sulfate reduction (SR)	$OM + \frac{1}{2}SO_4^{2-} \rightarrow CO_2 + \frac{1}{2}H_2S + \frac{121}{106}OH^-$	$R_{\min}\frac{K_{NO_3^-}}{K_{NO_3^-}+[NO_3^-]}\frac{K_{O_2}}{K_{O_2}+[O_2]}$
Nitrification (NIT)	$NH_4^+ + 2O_2 + 2OH^- \rightarrow NO_3^-$	$k_{\mathrm{NIT,max}}\frac{K_{NH_4^+}}{K_{NH_4^+}+[NH_4^+]}\frac{K_{O_2}}{K_{O_2}+[O_2]}$
Sulfide oxidation (Sox)	$H_2S + 2O_2 + 2OH^- \rightarrow SO_4^{2-}$	$k_{\mathrm{SOx,max}}\frac{K_{H_2S}}{K_{H_2S}+[H_2S]}\frac{K_{O_2}}{K_{O_2}+[O_2]}$
Calcium carbonate precipitation (CaP)	$Ca^{2+} + CO_2 + 2OH^- \rightarrow CaCO_3$	$\varphi k_{\mathrm{CaP}}\lvert\Omega_{CaCO_3} - 1\rvert^{n_{\mathrm{CaP}}}(\Omega_{CaCO_3} > 1)$
Calcium carbonate dissolution (CaD)	$CaCO_3 \rightarrow Ca^{2+} + CO_2 + 2OH^-$	$(1-\varphi)k_{\mathrm{CaD},1}[CaCO_3]\lvert\Omega_{CaCO_3} - 1\rvert^{n_{\mathrm{CaD}},1}(\Omega_{CaCO_3} > \Omega_{CaCO_3,\mathrm{crit}})$
		$(1-\varphi)k_{\mathrm{CaD},2}[CaCO_3]\lvert\Omega_{CaCO_3} - 1\rvert^{n_{\mathrm{CaD}},2}(\Omega_{CaCO_3} < \Omega_{CaCO_3,\mathrm{crit}})$

Note. OM = organic matter $(CH_2O \cdot (NH_3)_{\frac{16}{106}} \cdot (H_3PO_4)_{\frac{1}{106}})$, Alkalinity is depicted as OH^-. Reactions are not balanced with respect to water or phosphate, but phosphate is considered for the alkalinity production.

Table 3
Boundary Conditions Used in the Biogeochemical Sediment Model

		Value				
	Symbol	Validation	Meta-model	Units	Method	Refs
Height of sediment column	h	8.5, 18.5, 26.0	10	cm	A	Huettel et al. (1998 2014), Lunstrum and Berelson (2022)
Salinity	S	35	35	–	C	
Temperature	T	15	15	°C	C	
Porosity	φ	0.45	0.45	–	C	
Porewater residence time	PRT	1.8, 3.6, 5.4	5	h	A	Lunstrum and Berelson (2022), McGinnis et al. (2014), Precht et al. (2004), Santos et al. (2012)
Oxygen of the inflowing water	$[O_2]_{in}$	254	254	µM	C	
DIC of the inflowing water	$[DIC]_{in}$	Depends on pCO_2 and A_T	Depends on pCO_2 and A_T	µM	C	
A_T of the inflowing water	$A_{T,in}$	2,420, 1,700, 1,500, 500	2,260	µmol kg^{-1}	A	Lunstrum and Berelson (2022), Munida data
NO_3^- of the inflowing water	$[NO_3^-]_{in}$	10	10	µM	A	Middelburg et al. (1997)
NH_4^+ of the inflowing water	$[NH_4^+]_{in}$	0	0	µM	–	
H_2S of the inflowing water	$[H_2S]_{in}$	0	0	µM	–	
Mineralization rate	R_{min}	22	22	mmol m^{-2} d^{-1}	A	Rusch et al. (2006)
$CaCO_3$ concentration	$[CaCO_3]$	0.83	0–100	wt.% $CaCO_3$	A	Lunstrum and Berelson (2022)
Fraction of aragonite	$f_{aragonite}$	0.5	0.5	–	A	Lunstrum and Berelson (2022)
Atmospheric CO_2 concentration	pCO_2	424	320–1,500	ppm	A	

Note. *A* = Literature values, *B* = calibrated, *C* = calculated based on environmental parameters.

Table 4
Reaction Parameters Used in the Biogeochemical Sediment Model

	Symbol	Value	Units	Method	Refs
Half-saturation constant AR	K_{O2}	1	μM	A	Soetaert et al. (1996), van de Velde, Hidalgo-Martinez et al. (2020)
Half-saturation constant DN	K_{NO3}	5	μM	A	Soetaert et al. (1996) van de Velde, Hidalgo-Martinez et al. (2020)
Half-saturation constant NIT	K_{NH4}	5	μM	A	Soetaert et al. (1996)
Half-saturation constant SO_x	K_{H2S}	5	μM	A	Soetaert et al. (1996), van de Velde and Meysman (2016)
Max. nitrification rate	$k_{NIT,max.}$	100	μmol cm^{-3} yr^{-1}	A	Soetaert et al. (1996)
Max. sulfide oxidation rate	$k_{SOx,max.}$	100	μmol cm^{-3} yr^{-1}	A	Soetaert et al. (1996)
Calcite precipitation rate constant	k_{CaP}	0.4	μmol cm^{-3} yr^{-1}	A	Sulpis, Humphreys et al. (2022)
Calcite precipitation rate exponent	n_{CaP}	1.76	–	A	Sulpis, Humphreys et al. (2022)
Calcite dissolution rate constant	$k_{CaD,1}$	20	yr^{-1}	A	Sulpis, Humphreys et al. (2022)
	$k_{CaD,2}$	6.3 10^{-3}	yr^{-1}	A	Sulpis, Humphreys et al. (2022)
Calcite dissolution exponent	$n_{CaD,1}$	4.7	–	A	Sulpis, Humphreys et al. (2022)
	$n_{CaD,2}$	0.11	–	A	Sulpis, Humphreys et al. (2022)
Aragonite dissolution rate constant	$k_{ArD,1}$	4.2	yr^{-1}	A	Sulpis, Humphreys et al. (2022)
	$k_{ArD,2}$	0.1	yr^{-1}	A	Sulpis, Humphreys et al. (2022)
Aragonite dissolution rate exponent	$n_{ArD,1}$	1.46	–	A	Sulpis, Humphreys et al. (2022)
	$n_{ArD,2}$	0.13	–	A	Sulpis, Humphreys et al. (2022)
Critical calcite saturation	$\Omega_{cal,crit}$	0.828	–	A	Sulpis, Humphreys et al. (2022)
Critical aragonite saturation	$\Omega_{ara,crit}$	0.835	–	A	Sulpis, Humphreys et al. (2022)
Calcite equilibrium solubility product	$K_{SP}^{Calcite}$	4.31 10^{-7}	$(mol\ kg^{-1})^2$	C	
Aragonite equilibrium solubility product	$K_{SP}^{Aragonite}$	6.72 10^{-7}	$(mol\ kg^{-1})^2$	C	

Note. A = Literature values, B = calibrated, C = calculated based on environmental parameters.

production relative to the total DIC production (Figure 3b). Given the uncertainties in the experimental setup, data and model showed excellent agreement ($R^2 = 0.63$ for $CaCO_3$ dissolution and $R^2 = 0.59$ for A_T vs. DIC production), which suggests our seafloor model is well designed and able to simulate $CaCO_3$ dissolution in organic-matter poor sandy sediments. To create the meta-model, we set the sediment height at 10 cm, based on typical

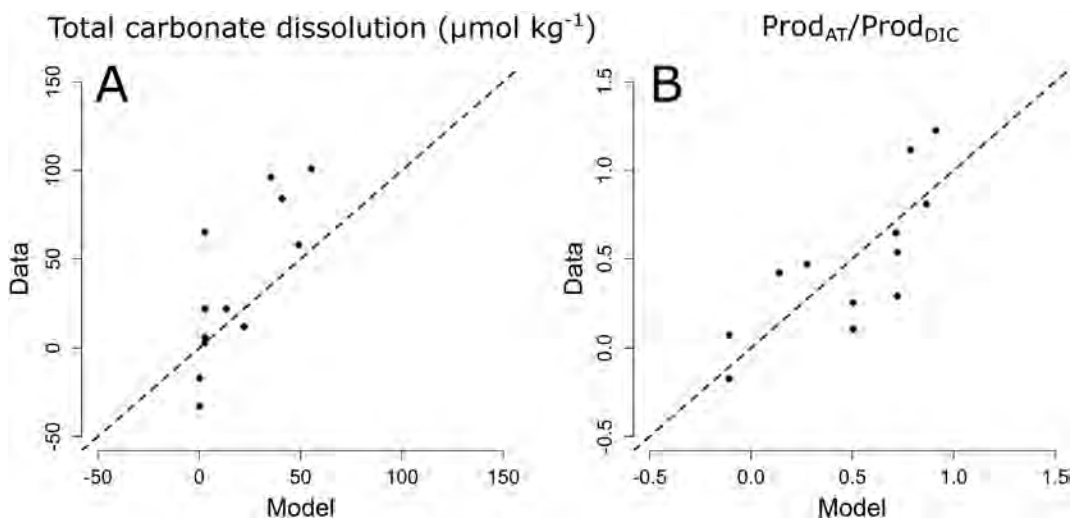

Figure 3. Shelf seafloor model validation. Comparison of the flow-through experiment of Lunstrum and Berelson (2022) with the model output. (a) Total amount of carbonate dissolved over the duration of the experiment. (b) Alkalinity (A_T) production relative to the dissolved inorganic carbon (DIC) production.

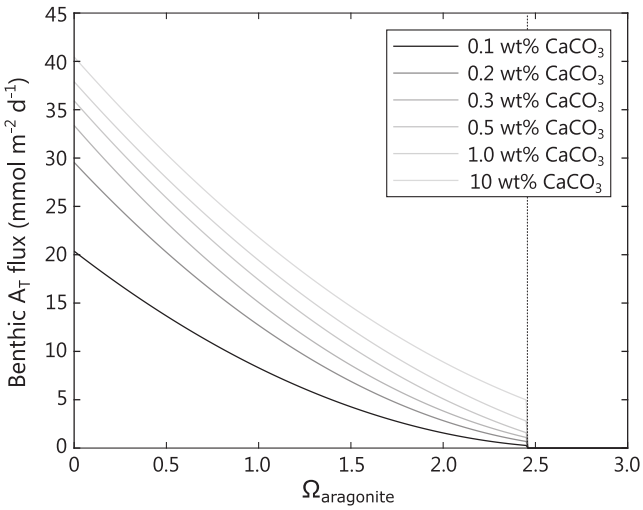

Figure 4. $\Omega_{aragonite}$ versus benthic A_T flux. The relationship between aragonite saturation state ($\Omega_{aragonite}$) and flux of alkalinity (A_T) released from sandy shelf seafloor sediments for different assumptions of initial wt.% $CaCO_3$. No additional A_T is released when $\Omega_{aragonite}$ exceeds 2.45 following (Lunstrum & Berelson, 2022).

flow fields in sandy sediments (Huettel et al., 1998). Water flowing into the sediment must also flow out, so a sediment height of 10 cm implies water circulation down to 5 cm depth. We expressed the $CaCO_3$ dissolution rate in volumetric units (μmol cm^{-3} yr^{-1}), which avoids double counting if we were to express it per surface area. We set the porewater residence time to 5h, which is a typical porewater residence time for sandy sediments (Lunstrum & Berelson, 2022; McGinnis et al., 2014; Precht et al., 2004; Santos et al., 2012). We kept the A_T of the inflowing water constant at the mean value measured at the shelf station of the Munida transect and varied the pCO_2 and $CaCO_3$ concentrations, which are the only two parameters that will vary in the box model of the east Otago shelf and are the key controls on seafloor $CaCO_3$ dissolution (Lunstrum & Berelson, 2022). We then used the model output to make a predictive relation:

$$R_{dissolution} = \begin{cases} a + b(\Omega_{aragonite}) + c(\Omega_{aragonite})^2 & \text{if } \Omega_{aragonite} \le 2.45 \\ 0 & \text{else} \end{cases} \quad (9)$$

where terms a, b, and c define the relation between A_T release and local benthic $\Omega_{aragonite}$ which depends on the assumed initial wt.% $CaCO_3$ of the shelves (Figure 4).

2.2.3. Experimental Design

To account for the uncertainty in the parameter sets, we set up a Monte Carlo approach where we randomly selected 10,000 parameter combinations within the limits given in Table 1. We ran the model to steady state for the year 1998 (the first year of the Munida time series). We subsequently filtered the results by only retaining those parameter combinations that gave steady-state A_T and $\Omega_{aragonite}$ that fell within the values measured during the Munida transect, as well as sediment $CaCO_3$ concentrations that agreed with the available data (Bostock et al., 2019; Carter, 1986; A. M. Smith et al., 2010). After this filtering step, we retained 89 unique parameter sets, which we subsequently forced with the atmospheric pCO_2 from 1998 to 2024. We repeated this experiment three times and produced a baseline run (fixed $CaCO_3$ dissolution in the seafloor, fixed calcification), a calcification-only run (fixed $CaCO_3$ dissolution in the seafloor, Ω-dependent calcification), and a full run (Ω-dependent $CaCO_3$ dissolution in the seafloor and calcification).

2.3. Earth System Model of Intermediate Complexity—"cGENIE"

To test the impact of anthropogenic CO_2 release and subsequent shelf $CaCO_3$ dissolution on ocean CO_2 uptake rates, we used the carbon-Grid ENabled Integrated Earth system model (cGENIE). cGENIE is a three-dimensional global model with representation of the atmosphere, ocean, marine biosphere, and seafloor sediments. Full model details, configuration settings, and experimental design are given in the Supplementary Information. The model includes a pelagic calcification feedback by calculating the ratio of $CaCO_3$ to particulate organic carbon (POC) export production as a function of the local surface ocean calcite saturation state (Ridgwell, Zondervan, et al., 2007). Remineralization of particles in the water column occurs along a fixed profile with depth representing exponential decay. All POC and $CaCO_3$ particles that reach the seafloor are instantaneously remineralized and returned to the ocean in a closed system set-up hence no interactive sediment $CaCO_3$ dissolution feedback is included here. The model is spun up for 20,000 years to reach equilibrium preindustrial conditions under atmospheric pCO_2 of 278 μatm (roughly equivalent to a xCO_2 of 278 ppm).

We ran the model for three Representative Concentration Pathways (RCP) scenarios, RCP1.9, RCP2.6, and RCP4.5. For each, a concentration-driven control simulation is run for 350 years with pCO_2 restored to historical values (Meinshausen et al., 2017) followed by their respective future prediction of pCO_2 between the years 1750 and 2100 (Meinshausen et al., 2020). Note that we applied a one-to-one conversion between xCO_2 (concentration of atmospheric CO_2 in moles of CO_2 of the total gas mixture) and pCO_2 (concentration of atmospheric CO_2 in partial pressure), an appropriate assumption in cGENIE where all physical and chemical ocean-atmosphere interactions occur at sea level where air pressure is 1 atm and pCO_2 equals xCO_2. Grid cells with depths shallower

than 558 m are potential locations where seafloor $CaCO_3$ dissolution could occur (Figure S3 in Supporting Information S1). The time-varying benthic $\Omega_{aragonite}$ at these sites is used to offline calculate the local release of A_T between 1,750 and 2,100 for initial $CaCO_3$ concentrations of 0.1, 0.2, 0.3, 0.5, 1.0, and 10.0 wt.% following Equation 9. The three RCP experiments with CO_2 restoring forcing are repeated but now include an added benthic flux forcing of A_T and DIC from carbonate-poor shelves, totaling 18 experiments with six different assumptions of initial wt.% $CaCO_3$ (Figure S4 in Supporting Information S1). The impact of A_T release on oceanic CO_2 uptake is reported as the difference in diagnosed CO_2 emissions required to track the RCP trajectories between the control and A_T release experiment.

Because pCO_2 is prescribed in the concentration-driven RCP experiments, the impact of benthic A_T release on pCO_2 is not considered. To investigate the implications of this method, an equivalent CO_2 flux-driven experiment is run for the most extreme scenario RCP4.5 in which the diagnosed CO_2 emission flux of the concentration-driven control experiment from 1750 to 2100 is applied as forcing. Here, pCO_2 varies freely as a result of the applied CO_2 flux, carbon cycle feedbacks, and the additional A_T release from sandy shelves. This reveals that the ocean CO_2 uptake may be overestimated in the concentration-driven experiment by ~0.01 Pg C yr^{-1} by year 2100 (Figure S5 in Supporting Information S1). The release of benthic A_T from the sandy shelves lowers pCO_2, so ocean CO_2 uptake is mitigated compared to the concentration-driven experiment. Nonetheless, we report results of the concentration-driven experiment from which the benthic A_T release fluxes are derived for consistency.

3. Results and Discussion

3.1. Seafloor Carbonate Dissolution Drives Shelf Alkalinity Increase

The time series data of the shelf site shows higher variability than the subantarctic data, in particular the A_T (Figure 5). This is not unexpected, as nearshore waters are more strongly influenced by short-term events such as changes in riverine input, are more rapidly affected by changes in seafloor geochemistry, and are impacted more directly by anthropogenic activities. Our data analysis shows continuous declining $\Omega_{aragonite}$ at both the shelf (-0.012 ± 0.001 per year) and subantarctic station (-0.009 ± 0.001 per year) (Figure 5a, Table S1 in Supporting Information S1). At the same time, there is an increase in A_T at the shelf station of 0.65 ± 0.25 μmol kg^{-1} per year, whereas the subantarctic station shows no significant change (slope 0.00 ± 0.07 μmol kg^{-1} per year), suggesting a systematic difference between the shelf and open ocean site (Figure 5b, Table S1 in Supporting Information S1). This increase in shelf A_T may have three possible causes: (a) increasing on-shelf entrainment of modified subtropical waters of higher A_T, (b) increasing A_T delivery from rivers, or (c) changing local A_T consumption/production processes. We assess these three possibilities below.

The more saline modified subtropical water over the mid- to outer-shelf (30–150 m water depth; Figure 1) originates from the Tasman Sea, having flowed poleward then northeastward around southern Aotearoa New Zealand in a counterclockwise direction (R. O. Smith et al., 2013; P. J. H. Sutton, 2003). An intensification of this flow has been suggested based on significant warming of sea-surface temperature observed around the southern coast of Aotearoa New Zealand over the last half-century (Shears & Bowen, 2017). However, no current measurements are available to determine whether the modified subtropical water flow has steadily increased over time. Modified subtropical water is known to be entrained by the inner-shelf (<30 m water depth) via a range of cross-shelf transport mechanisms, including wind-driven up- and down-welling (Johnson et al., 2023) and also a large headland eddy in the lee of the Otago Peninsula (Murdoch, 1989). To account for the potential influence modified subtropical water entrainment at the shelf station, we normalized the measured A_T to the measured salinity to account for any mixing with higher salinity (and A_T) waters. This normalization reduced the slope by about 50% to 0.28 ± 0.24 μmol kg^{-1} per year (Table S1 in Supporting Information S1), indicative of some influence of increasing on-shelf entrainment. Note that the alkalinity content of the subtropical water remained quasi-constant in A_T over the duration of the time series (Figure S6 and Table S1 in Supporting Information S1).

Increased riverine A_T delivery has been reported for the Mississippi and several rivers on the east coast of the United States, as well as in large rivers in the Russian Arctic (Drake et al., 2018; Kaushal et al., 2013; Najjar et al., 2020; Raymond & Cole, 2003). The causes of this increase vary and have been linked to increases in riverine discharge (Drake et al., 2018; Raymond & Cole, 2003), increased weathering of carbonate rocks due to elevated acid deposition (Kaushal et al., 2013), and decreases in estuarine calcification rates (Najjar et al., 2020). The two main rivers discharging onto the east Otago shelf are the Clutha (mean discharge ~574 m^3 s^{-1}) and the Taieri (mean discharge ~36 m^3 s^{-1}) (Otago Regional Council, 2025), both of which drain a terrain of greywacke

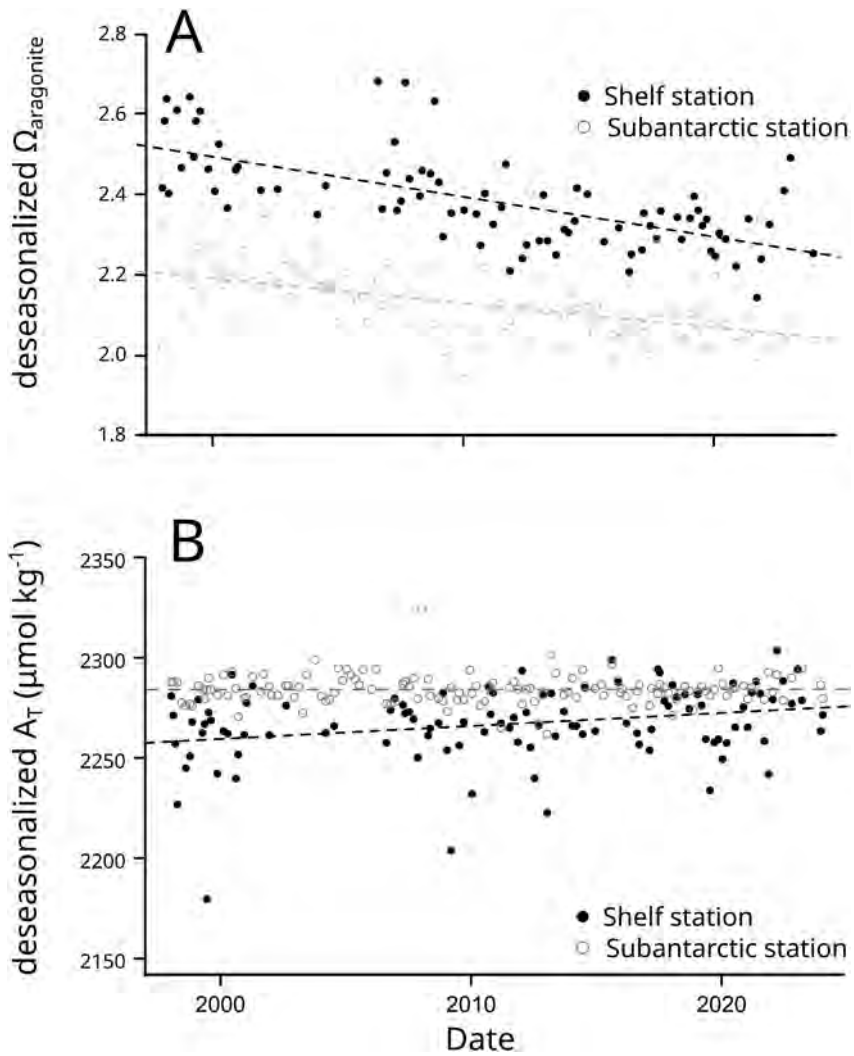

Figure 5. Munida time series. Surface water (~5 m water depth) trends at the continental shelf and subantarctic stations for (a) aragonite saturation state ($\Omega_{aragonite}$), and (b) alkalinity (A_T). Trendlines and uncertainties have been derived following best practices outlined in A. J. Sutton et al. (2022).

deposits, which is composed of quartz and sandstone with high amounts of silt and clay (Kautz & Martin, 2007). This bedrock does not weather efficiently, as is shown by the low A_T content of these rivers (500–600 µmol kg^{-1}) (Kim et al., 1996; Kim & Hunter, 2001), which did not vary between 1989 and 2025 (Table S2 in Supporting Information S1). Furthermore, there has been no significant change in riverine discharge between 2000 and 2024 for either river (Otago Regional Council, 2025), and so it is unlikely that the A_T increase observed on the east Otago shelf is driven by increased riverine delivery.

The third option is a change in the balance between A_T producing and consuming processes on the east Otago shelf. The calcification rate of most calcifying organisms is dependent on Ω of the surrounding water (Gattuso et al., 1999; Leclercq et al., 2002; Lehmann & Bach, 2025). At the same time, $CaCO_3$ dissolution in low carbonate and organic-matter poor sandy sediments, such as on the east Otago shelf (Bostock et al., 2019; Carter, 1986), is controlled by the Ω of the overlying water (Lunstrum & Berelson, 2022). Accordingly, we hypothesize that increasing levels of atmospheric CO_2 and the resultant decreasing Ω simultaneously reduce the calcification rate whilst stimulating seafloor $CaCO_3$ dissolution, leading to an increase in shelf A_T. Our box model results demonstrate that the combined effects of reduced water-column calcification and increased seafloor $CaCO_3$ dissolution, in response to increasing atmospheric and seawater CO_2, can explain the majority of the observed A_T trend on the east Otago shelf (Figure 6). Over the timescale of the model experiment, the change in benthic $CaCO_3$

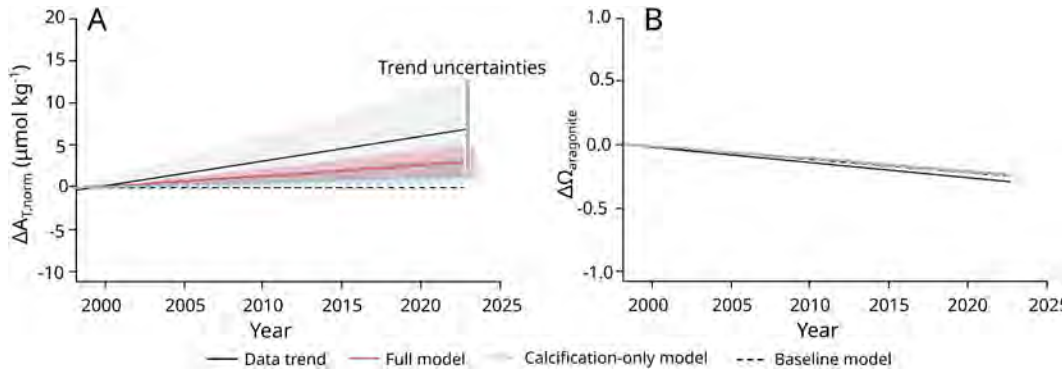

Figure 6. Comparison of the observed data trend (black line, gray shaded area is standard error) to modeled trends from box model simulations for the Otago shelf with fixed calcification and fixed $CaCO_3$ dissolution in the seafloor (baseline model, dashed line), with Ω-dependent calcification and fixed $CaCO_3$ dissolution in the seafloor (calcification-only model, blue line and shading), with Ω-dependent calcification and $CaCO_3$ dissolution in the seafloor (full model, red line and shading) for (a) shelf alkalinity, normalized to salinity ($\Delta A_{T,norm}$), and (b) aragonite saturation state ($\Delta\Omega_{aragonite}$). Model uncertainty was derived by a Monte Carlo simulation of all plausible parameter combinations (see text for more details).

stock was negligible, and calcification was always higher than dissolution, which indicates that seafloor $CaCO_3$ will likely not be a limiting factor for benthic A_T production. Our model does not account for increases in OM supply to the seafloor, which can increase seafloor $CaCO_3$ dissolution rate by increasing porewater acidification (Andersson et al., 2003; Morse & Mackenzie, 1990). While there is not enough data available to constrain the potential increase in seafloor OM mineralization, a recent assessment of changes in marine primary productivity over 1998–2022, as measured by remotely-sensed Chlorophyll-a concentrations, show a significant increase in Chl-a along the southern South Island in both the subtropical waters over the shelf and the offshore subantarctic seawater of New Zealand of 5%–10% per decade (Pinkerton et al., 2024). Hence, it is likely the shelf has seen an increase in seafloor organic mineralization in the last 25 years, which implies our results may underestimate shelf $CaCO_3$ dissolution rates, which could explain the stronger increase in shelf A_T in the data compared to the model.

3.2. Assessing the Potential for a Fast Climate Feedback From Shelf Seafloor Carbonate Dissolution

As >60% of the continental shelf seafloor consists of sediments with low concentrations of $CaCO_3$ and OM, comparable to those of the east Otago shelf (Milliman, 1993), it is possible that a similar seafloor dissolution feedback occurs in shelf waters across the global oceans. Indeed, regions with muddy seafloors showed no significant trend in A_T in the overlying water (Figure 7a), whereas shelf systems with sandy seafloors, such as in the North Atlantic, Mediterranean, and south Pacific (Figures 7b–7d), show increasing shelf A_T in line with decreasing $CaCO_3$ saturation states (Table S1 in Supporting Information S1). Furthermore, increasing A_T has also been observed in the global surface ocean (Barrett et al., 2025) with an estimated global mean increase in A_T is around 0.1 µmol kg^{-1} yr^{-1} over the past 30 year, mainly attributed to reduced water column calcification (Barrett et al., 2025). This is far less than what we observe in shelf waters (0.3–1.0 µmol kg^{-1} yr^{-1}; Table S1 in Supporting Information S1) and suggests the influence of other processes in nearshore waters. The response of near-shore waters may be more intense due to the closer connection with the seafloor, so the response of seafloor $CaCO_3$ dissolution to reducing Ω would lead to higher A_T directly in the water column. These global observations suggest that the increase in shelf seafloor $CaCO_3$ dissolution driven by increasing atmospheric CO_2 we observe on the east Otago shelf is a potential global phenomenon.

To obtain a first-order estimate of the impact of the shelf seafloor carbonate dissolution feedback, we assume that the response of global sandy shelf seafloors to anthropogenic Ω change is similar to the east Otago shelf. On a global scale, enhanced carbonate dissolution in the shelf seafloor would then result in an additional release of 5–13 Tmol A_T yr^{-1} over the last 25 years, assuming the increase in areal $CaCO_3$ dissolution is identical in across the global sandy shelf. Currently, global shallow seafloor $CaCO_3$ dissolution is estimated to release 54 Tmol A_T yr^{-1} (van de Velde et al., 2025), and so our results suggest that 10%–25% of could be caused by the anthropogenically induced enhanced shelf seafloor carbonate. If all this excess A_T would re-equilibrate with the atmosphere, we expect an increase in ocean uptake of 0.05–0.13 Pg C yr^{-1} (assuming 0.84 mol of CO_2 uptake per mole of A_T addition;

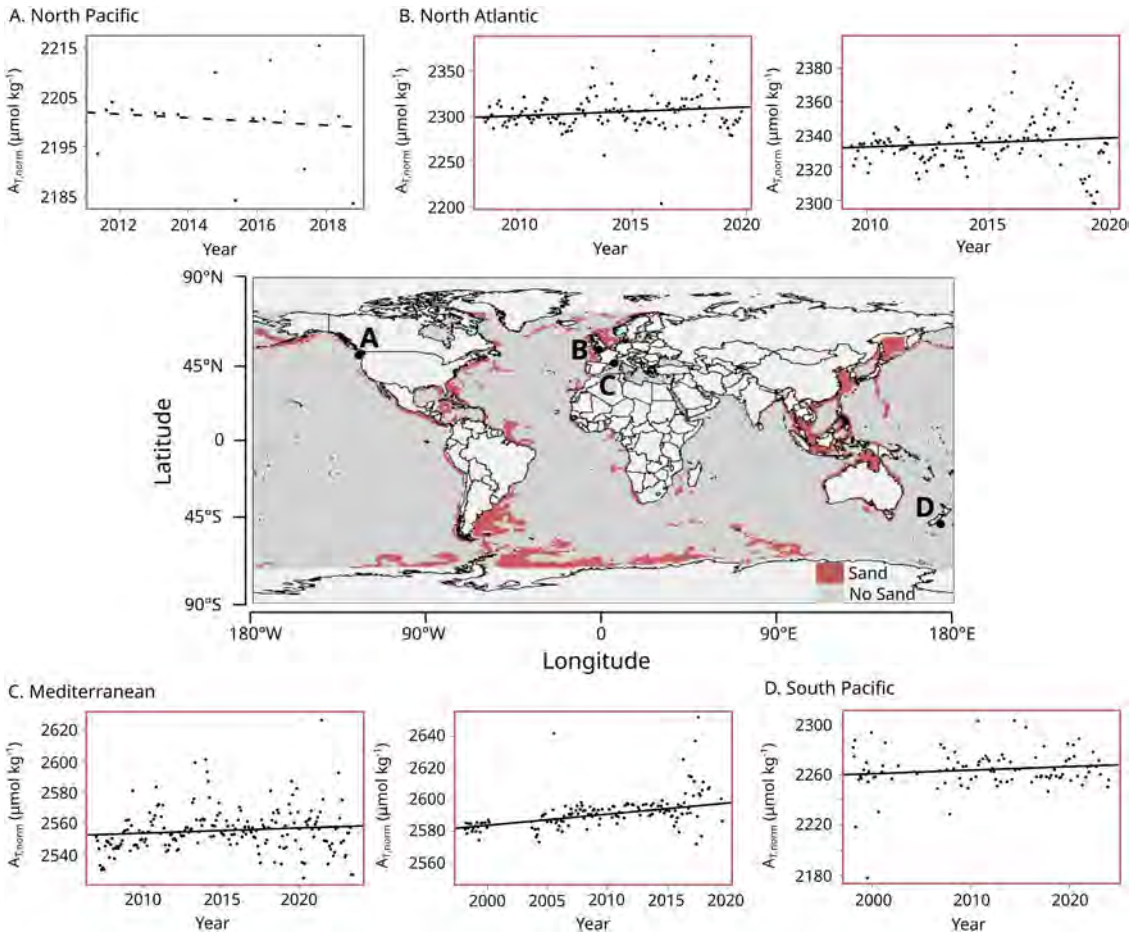

Figure 7. Compilation of global shelf alkalinity time series. Alkalinity ($A_{T,norm}$) are normalized to salinity and deseasonalized. Positive trends are indicated with a solid trendline, negative correlations with a dashed trendline. Trends have been determined following the best practices for time series analysis (A. J. Sutton et al., 2022), statistics are summarized in Table S1 in Supporting Information S1. Red figure border indicates that the field site has predominantly sandy sediments, and a gray figure border indicates predominantly muddy or siliclastic sediments. (a) Time series from the Salish sea, connected to the North Pacific (Alin et al., 2024). (b) Two time series from the northern French coast, connected to the North Atlantic (Metzl et al., 2024). (c) Two time series from the Mediterranean sea (Kapsenberg et al., 2017; Metzl et al., 2024). (d) Time series from the east coast of Aotearoa New Zealand, connected to the South Pacific and Southern Ocean (this study).

Frankignoulle, 1994). This extra CO_2 uptake could account for 15%–40% of the 0.3 Pg C yr^{-1} offset between global ocean models and data products.

However, since some of the A_T will be released in regions with predominantly downwelling conditions, or in deeper parts of the shelf, not all the A_T-enriched shelf water will equilibrate with the atmosphere on centennial timescales. Additionally, the CO_2 uptake efficiency per mole of A_T addition is dependent on the A_T and DIC as well as on salinity and temperature (Frankignoulle, 1994), all of which will vary in response to anthropogenic forcing. To generate a more realistic estimate of the potential importance of the shelf seafloor carbonate dissolution feedback on a global scale, we use the EMIC cGENIE, which was specifically designed to simulate carbon cycle feedbacks and ocean circulation dynamics on a variety of timescales (Cao et al., 2009; Vervoort et al., 2019). Our model simulations suggest that the seafloor carbonate dissolution feedback leads to additional uptake of 0.015–0.033 Pg C yr^{-1} in 2025, and up to 0.085 Pg C yr^{-1} in the year 2100 for RCP4.5 (Figure 8). The rates are about 70% lower than when assuming a fixed relation between global A_T and DIC increases and ocean uptake rates. Two main factors explain this difference. First, the box model assumes that all released shelf A_T resurfaces and equilibrates instantaneously, whereas in cGENIE the average transit time is ∼50 years, that is, the full effect of the enhanced A_T release has not yet emerged by 2100. In addition, some of the shelf A_T flux is transported to the deep ocean and does not affect CO_2 uptake rates on the centennial timescales simulated here. Second, in contrast to the box model, cGENIE resolves spatial variability in carbonate chemistry, surface

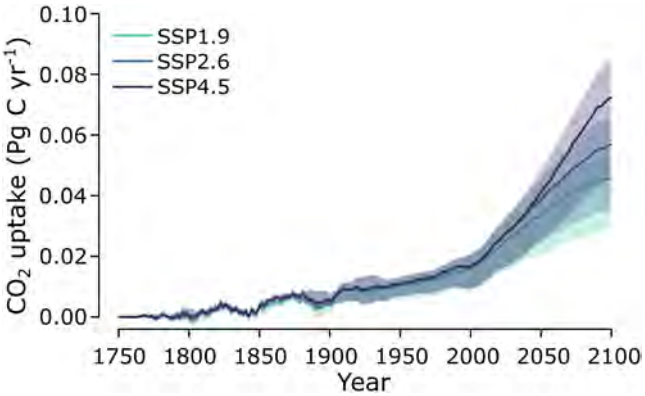

Figure 8. Simulated increase in global ocean CO_2 uptake from 1750 to 2100 from shelf seafloor carbonate dissolution in the cGENIE Earth System model of intermediate complexity for three Representative Concentration Pathways. Shaded area in both panels indicate the range of model results (see Section 2).

temperature, and salinity and so the impact of A_T release depends on the geographical location and depth where it is released. The effect is further modified by nonlinear carbon cycle feedbacks in cGENIE such as CO_2 solubility, carbon speciation, saturation-state dependent CaCO3:POC export ratio, and physical ocean ventilation processes. Despite the reduced resolution, our EMIC demonstrates that benthic A_T release in shallow environments may indeed have an impact on CO_2 uptake on annual-decadal timescales.

Inclusion of the carbonate-poor shelf seafloor carbonate dissolution feedback could explain ∼10% of the model-data mismatch in estimates of ocean CO_2 uptake rates. The remaining mismatch is possibly due to other processes that increase ocean alkalinity that are also not represented in Earth-system models, such as the decline in carbonate production of coral reefs (Cornwall et al., 2021; Kwiatkowski et al., 2025). Additionally, the reduced model resolution likely underestimates the total impact, since the grid cells assume to release A_T from the shelf seafloor in cGENIE have a combined area of 10.23 million km^2, which is only ∼60% of the carbonate-poor shelf area. In this simulation, we assumed that $CaCO_3$ dissolution in the global carbonate-poor shelf area has the same sensitivity to reducing saturation state as we observe on the Otago shelf. It is unlikely this is fully accurate, and other factors, such as changes in circulation or riverine input, could contribute to the observed increase in A_T identified at other shelves. Further research into the local dynamics of individual shelf locations and longer monitoring time series are needed to build a more complete picture of the global impact of shelf $CaCO_3$ dissolution. Nevertheless, our estimate demonstrates that benthic A_T release in shallow environments can have an important impact on CO_2 uptake on annual-decadal timescales. Models with a higher-resolution representation of the seafloor are required to obtain more accurate estimates of the seafloor area impacted by this feedback, including a comparison of the spatial distribution to the divergence of the model-data mismatch in the global carbon budget.

The potential existence of this fast feedback not only challenges our understanding of carbon cycle feedbacks and represents a potential blind spot in current climate modeling but also has major implications for the deployment of ocean alkalinity enhancement as a carbon dioxide removal technology (Renforth & Henderson, 2017). For example, an increase in ocean alkalinity resulting from deliberate addition would increase the Ω of the ocean waters and decrease shelf seafloor $CaCO_3$ dissolution rates. Together with the potential increase in calcification rates (Barrett et al., 2025; Gattuso et al., 1999; Leclercq et al., 2002; Lehmann & Bach, 2025), this implies that any deliberate addition of A_T to the ocean will be balanced by an increase in net $CaCO_3$ production. As a result, any deployment of ocean alkalinity enhancement will need to consider the shelf seafloor $CaCO_3$ feedback in estimates of the total impact on ocean CO_2 uptake rates. For example, current upper estimates of ocean alkalinity enhancement in coastal and shelf waters are on the order of 30 Tmol A_T yr^{-1}, which would lead to an increase in CO_2 uptake of ∼0.3 Pg C yr^{-1} (Palmiéri & Yool, 2024). While this number is not constrained by any practical limitations and thus almost certainly an overestimate, our estimates suggest that ∼10–25% of this enhanced uptake would be offset by inhibition of natural alkalinity sources if deployed in 2100.

4. Conclusions

There is evidence that anthropogenic CO_2 emissions have started to increase deep-sea $CaCO_3$ dissolution rates (J. D. Müller & Gruber, 2024; Sulpis et al., 2018). This long-term feedback will eventually lead to increased CO_2 uptake on timescales of 1,000 years or longer (Archer, 2005). Data from the east Otago shelf suggests that the response of shelf seafloor $CaCO_3$ dissolution to rising atmospheric CO_2 and surface ocean acidification acts more rapidly on annual-decadal timescales and thus constitutes a fast climate feedback. Upscaling our results to the global shelf seafloor indicates that this fast shelf seafloor feedback would limit the efficiency of any deliberate additions of alkalinity to stimulate oceanic CO_2 uptake, and future experiments should confirm the presence of this feedback in the global shelf seafloor. These results highlight the value of long-term monitoring time series for better understanding how the natural marine carbonate system is responding to anthropogenic CO_2 emissions, which is critical for determining the response to potential climate intervention techniques.

Conflict of Interest

The authors declare no conflicts of interest relevant to this study.

Data Availability Statement

All novel data presented in this manuscript is available via https://doi.org/10.5281/zenodo.17517517 (van de Velde, 2025a). The model code is available via https://doi.org/10.5281/zenodo.17508535 (van de Velde, 2025b).

Acknowledgments
The authors would like to thank the captain and crew of the RV Munida and RV Polaris II for support during the fieldwork, and Judith Murdoch for support with the laboratory analyses. SJv, CSL, and KC acknowledge the New Zealand MBIE Strategic Science Investment Fund for supporting the Munida transect via the NIWA Ocean-Climate Interaction programme. PV acknowledges support from the Natural Environment Research Council (UK) award NE/W009625/1.

References

Albright, R., Caldeira, L., Hosfelt, J., Kwiatkowski, L., Maclaren, J. K., Mason, B. M., et al. (2016). Reversal of ocean acidification enhances net coral reef calcification. *Nature*, *531*(7594), 362–365. https://doi.org/10.1038/nature17155

Alin, S. R., Newton, J. A., Feely, R. A., Greeley, D., Curry, B., Herndon, J., & Warner, M. (2024). A decade-long cruise time series (2008–2018) of physical and biogeochemical conditions in the southern Salish Sea, North America. *Earth System Science Data*, *16*(2), 837–865. https://doi.org/10.5194/essd-16-837-2024

Aller, R. C. (1982). Carbonate dissolution in nearshore terrigenous muds: The role of physical and biological reworking. *The Journal of Geology*, *90*(1), 79–95. https://doi.org/10.1086/628652

Andersson, A. J., Mackenzie, F. T., & Lerman, A. (2006). Coastal ocean CO2–carbonic acid–carbonate sediment system of the Anthropocene. *Global Biogeochemical Cycles*, *20*(1). https://doi.org/10.1029/2005GB002506

Andersson, A. J., Mackenzie, F. T., & Ver, L. M. (2003). Solution of shallow-water carbonates: An insignificant buffer against rising atmospheric CO_2. *Geology*, *31*(6), 513–516. https://doi.org/10.1130/0091-7613(2003)031<0513:SOSCAI>2.0.CO;2

Archer, D. (2005). Fate of fossil fuel CO_2 in geologic time. *Journal of Geophysical Research*, *110*(C9). https://doi.org/10.1029/2004JC002625

Barrett, R. C., Carter, B. R., Fassbender, A. J., Tilbrook, B., Woosley, R. J., Azetsu-Scott, K., et al. (2025). Biological responses to Ocean acidification are changing the Global Ocean carbon cycle. *Global Biogeochemical Cycles*, *39*(3), e2024GB008358. https://doi.org/10.1029/2024GB008358

Berner, R. A. (1991). A model for atmospheric CO2 over phanerozoic time. *American Journal of Science*, *261*(4), 339–376. https://doi.org/10.2475/ajs.291.4.339

Bostock, H., Jenkins, C., Mackay, K., Carter, L., Nodder, S., Orpin, A., et al. (2019). Distribution of surficial sediments in the ocean around New Zealand/Aotearoa. Part B: Continental shelf. *New Zealand Journal of Geology and Geophysics*, *62*(1), 24–45. https://doi.org/10.1080/00288306.2018.1523199

Boudreau, B. P. (1996). The diffusive tortuosity of fine-grained unlithified sediments. *Geochimica et Cosmochimica Acta*, *60*(16), 3139–3142. https://doi.org/10.1016/0016-7037(96)00158-5

Boudreau, B. P. (1997). *Diagenetic models and their implementation*. Springer-Verlag Berlin Heidelberg.

Boudreau, B. P., Middelburg, J. J., Hofmann, A. F., & Meysman, F. J. R. (2010). Ongoing transients in carbonate compensation. *Global Biogeochemical Cycles*, *24*(4), 1–13. https://doi.org/10.1029/2009GB003654

Cao, L., Eby, M., Ridgwell, A., Caldeira, K., Archer, D., Ishida, A., et al. (2009). The role of ocean transport in the uptake of anthropogenic CO2. *Biogeosciences*, *6*(3), 375–390. https://doi.org/10.5194/bg-6-375-2009

Carter, L. (1986). A budget for modern-holocene sediment on the South Otago continental shelf. *New Zealand Journal of Marine & Freshwater Research*, *20*(4), 665–676. https://doi.org/10.1080/00288330.1986.9516187

Chiswell, S. M., Bostock, H. C., Sutton, P. J. H., & Williams, M. J. (2015). Physical oceanography of the deep seas around New Zealand: A review. *New Zealand Journal of Marine & Freshwater Research*, *49*(2), 286–317. https://doi.org/10.1080/00288330.2014.992918

Cornwall, C. E., Comeau, S., Kornder, N. A., Perry, C. T., van Hooidonk, R., DeCarlo, T. M., et al. (2021). Global declines in coral reef calcium carbonate production under ocean acidification and warming. *Proceedings of the National Academy of Sciences*, *118*(21), e2015265118. https://doi.org/10.1073/pnas.2015265118

Currie, K. I., Macaskill, B., Reid, M. R., & Law, C. S. (2011). Processes governing the carbon chemistry during the SAGE experiment. *Deep Sea Research Part II: Topical Studies in Oceanography*, *58*(6), 851–860. https://doi.org/10.1016/j.dsr2.2010.10.023

Currie, K. I., Reid, M. R., & Hunter, K. A. (2011). Interannual variability of carbon dioxide drawdown by subantarctic surface water near New Zealand. *Biogeochemistry*, *104*(1), 23–34. https://doi.org/10.1007/s10533-009-9355-3

Dickson, A. G., Sabine, C. L., & Christian, J. R. (2007). *Guide to best practices for ocean CO2 measurements* (Vol. 3, pp. 1–191). PICES Special Publication.

Drake, T. W., Tank, S. E., Zhulidov, A. V., Holmes, R. M., Gurtovaya, T., & Spencer, R. G. M. (2018). Increasing alkalinity export from large Russian arctic Rivers. *Environmental Science & Technology*, *52*(15), 8302–8308. https://doi.org/10.1021/acs.est.8b01051

Eyre, B. D., Cyronak, T., Drupp, P., De Carlo, E. H., Sachs, J. P., & Andersson, A. J. (2018). Coral reefs will transition to net dissolving before end of century. *Science*, *359*(6378), 908–911. https://doi.org/10.1126/science.aao1118

Frankignoulle, M. (1994). A complete set of buffer factors for acid/base CO_2 system in seawater. *Journal of Marine Systems*, *5*(2), 111–118. https://doi.org/10.1016/0924-7963(94)90026-4

Friedlingstein, P., O'Sullivan, M., Jones, M. W., Andrew, R. M., Hauck, J., Landschützer, P., et al. (2025). Global Carbon Budget 2024. *Earth System Science Data*, *17*(3), 965–1039. https://doi.org/10.5194/essd-17-965-2025

Gattuso, J. P., Allemand, D., & Frankignoulle, M. (1999). Photosynthesis and calcification at cellular, organismal and community levels in coral reefs: A review on interactions and control by Carbonate Chemistry. *American Zoologist*, *39*(1), 160–183. https://doi.org/10.1093/icb/39.1.160

Gattuso, J. P., Epitalon, J.-M., Lavigne, H., Orr, J., Gentili, B., Hagens, M., et al. (2024). Seacarb: Seawater Carbonate Chemistry (Version 3.3.3). Retrieved from https://cran.r-project.org/web/packages/seacarb/index.html

Gattuso, J. P., Frankignoulle, M., Bourge, I., Romaine, S., & Buddemeier, R. W. (1998). Effect of calcium carbonate saturation of seawater on coral calcification. *Global and Planetary Change*, *18*(1), 37–46. https://doi.org/10.1016/S0921-8181(98)00035-6

Hönisch, B., Ridgwell, A., Schmidt, D. N., Thomas, E., Gibbs, S. J., Sluijs, A., et al. (2012). The geological record of ocean acidification. *Science*, *335*(6072), 1058–1063. https://doi.org/10.1126/science.1208277

Hopkins, J., Shaw, A. G. P., & Challenor, P. (2010). The Southland Front, New Zealand: Variability and ENSO correlations. *Continental Shelf Research*, *30*(14), 1535–1548. https://doi.org/10.1016/j.csr.2010.05.016

Hu, X., & Cai, W.-J. (2011). An assessment of ocean margin anaerobic processes on oceanic alkalinity budget. *Global Biogeochemical Cycles*, *25*(3), GB3003. https://doi.org/10.1029/2010GB003859

Huettel, M., Berg, P., & Kostka, J. E. (2014). Benthic exchange and biogeochemical cycling in permeable sediments. *Annual Review of Marine Science*, *6*(6), 23–51. https://doi.org/10.1146/annurev-marine-051413-012706

Huettel, M., Ziebis, W., Forster, S., & Luther, G. W. (1998). Advective transport affecting metal and nutrient distributions and interfacial fluxes in permeable sediments. *Geochimica et Cosmochimica Acta*, *62*(4), 613–631. https://doi.org/10.1016/S0016-7037(97)00371-2

Johnson, E. E., Collins, C., Suanda, S. H., Wing, S. R., Currie, K. I., Vance, J., & Smith, R. O. (2024). Drivers of neritic water intrusions at the subtropical front along a narrow shelf. *Continental Shelf Research*, *277*, 105248. https://doi.org/10.1016/j.csr.2024.105248

Johnson, E. E., Suanda, S. H., Wing, S. R., Currie, K. I., & Smith, R. O. (2023). Episodic summer Chlorophyll-a blooms driven by along-front winds at aotearoa's Southeast Shelf break front. *Journal of Geophysical Research: Oceans*, *128*(7), e2022JC019609. https://doi.org/10.1029/2022JC019609

Jones, D. C., Ito, T., Takano, Y., & Hsu, W.-C. (2014). Spatial and seasonal variability of the air-sea equilibration timescale of carbon dioxide. *Global Biogeochemical Cycles*, *28*(11), 1163–1178. https://doi.org/10.1002/2014GB004813

Jones, K. N., Currie, K. I., McGraw, C. M., & Hunter, K. A. (2013). The effect of coastal processes on phytoplankton biomass and primary production within the near-shore Subtropical Frontal Zone. *Estuarine, Coastal and Shelf Science*, *124*, 44–55. https://doi.org/10.1016/j.ecss.2013.03.003

Kapsenberg, L., Alliouane, S., Gazeau, F., Mousseau, L., & Gattuso, J. P. (2017). Coastal ocean acidification and increasing total alkalinity in the northwestern Mediterranean Sea. *Ocean Science*, *13*(3), 411–426. https://doi.org/10.5194/os-13-411-2017

Kaushal, S. S., Likens, G. E., Utz, R. M., Pace, M. L., Grese, M., & Yepsen, M. (2013). Increased River alkalinization in the Eastern U.S. *Environmental Science & Technology*, *47*(18), 10302–10311. https://doi.org/10.1021/es401046s

Kautz, C. Q., & Martin, C. E. (2007). Chemical and physical weathering in New Zealand's Southern Alps monitored by bedload sediment major element composition. *Applied Geochemistry*, *22*(8), 1715–1735. https://doi.org/10.1016/j.apgeochem.2007.03.031

Kessler, A. J., Rogers, A., Cyronak, T., Bourke, M. F., Hasler-Sheetal, H., Glud, R. N., et al. (2020). Pore water conditions driving calcium carbonate dissolution in reef sands. *Geochimica et Cosmochimica Acta*, *279*, 16–28. https://doi.org/10.1016/j.gca.2020.04.001

Kim, J. P., & Hunter, K. A. (2001). Geochemical cycling of major and minor elements in the Taieri River and Waipori River catchments. *Journal of the Royal Society of New Zealand*, *31*(4), 745–762. https://doi.org/10.1080/03014223.2001.9517672

Kim, J. P., Reid, M. R., Cunninghame, R. G., & Hunter, K. A. (1996). Aqueous chemistry of major ions and trace metals in the Clutha River, New Zealand. *Marine and Freshwater Research*, *47*(7), 919–928. https://doi.org/10.1071/mf9960919

Kwiatkowski, L., Planchat, A., Pyolle, M., Torres, O., Bouttes, N., Comte, A., & Bopp, L. (2025). Declining coral calcification to enhance twenty-first-century ocean carbon uptake by gigatonnes. *Proceedings of the National Academy of Sciences*, *122*(23), e2501562122. https://doi.org/10.1073/pnas.2501562122

Leclercq, N., Gattuso, J. P., & Jaubert, J. (2002). Primary production, respiration, and calcification of a coral reef mesocosm under increased CO2 partial pressure. *Limnology & Oceanography*, *47*(2), 558–564. https://doi.org/10.4319/lo.2002.47.2.0558

Lehmann, N., & Bach, L. T. (2025). Global carbonate chemistry gradients reveal a negative feedback on ocean alkalinity enhancement. *Nature Geoscience*, *18*(3), 1–7. https://doi.org/10.1038/s41561-025-01644-0

Liu, X., Dunne, J. P., Stock, C. A., Harrison, M. J., Adcroft, A., & Resplandy, L. (2019). Simulating water residence time in the coastal Ocean: A global perspective. *Geophysical Research Letters*, *46*(23), 13910–13919. https://doi.org/10.1029/2019GL085097

Lueker, T. J., Dickson, A. G., & Keeling, C. D. (2000). Ocean pCO_2 calculated from dissolved inorganic carbon, alkalinity, and equations for $K1$ and $K2$: Validation based on laboratory measurements of CO_2 in gas and seawater at equilibrium. *Marine Chemistry*, *70*(1), 105–119. https://doi.org/10.1016/S0304-4203(00)00022-0

Lunstrum, A., & Berelson, W. (2022). $CaCO_3$ dissolution in carbonate-poor shelf sands increases with ocean acidification and porewater residence time. *Geochimica et Cosmochimica Acta*, *329*, 168–184. https://doi.org/10.1016/j.gca.2022.04.031

McCandliss, R. R., Jones, S. E., Hearn, M., Latter, R., & Jago, C. F. (2002). Dynamics of suspended particles in coastal waters (southern North Sea) during a spring bloom. *Journal of Sea Research*, *47*(3), 285–302. https://doi.org/10.1016/S1385-1101(02)00123-5

McGinnis, D. F., Sommer, S., Lorke, A., Glud, R. N., & Linke, P. (2014). Quantifying tidally driven benthic oxygen exchange across permeable sediments: An aquatic eddy correlation study. *Journal of Geophysical Research: Oceans*, *119*(10), 6918–6932. https://doi.org/10.1002/2014JC010303

Meinshausen, M., Nicholls, Z. R. J., Lewis, J., Gidden, M. J., Vogel, E., Freund, M., et al. (2020). The shared socio-economic pathway (SSP) greenhouse gas concentrations and their extensions to 2500. *Geoscientific Model Development*, *13*(8), 3571–3605. https://doi.org/10.5194/gmd-13-3571-2020

Meinshausen, M., Vogel, E., Nauels, A., Lorbacher, K., Meinshausen, N., Etheridge, D. M., et al. (2017). Historical greenhouse gas concentrations for climate modelling (CMIP6). *Geoscientific Model Development*, *10*(5), 2057–2116. https://doi.org/10.5194/gmd-10-2057-2017

Metzl, N., Fin, J., Lo Monaco, C., Mignon, C., Alliouane, S., Antoine, D., et al. (2024). A synthesis of ocean total alkalinity and dissolved inorganic carbon measurements from 1993 to 2022: The SNAPO-CO2-v1 dataset. *Earth System Science Data*, *16*(1), 89–120. https://doi.org/10.5194/essd-16-89-2024

Middelburg, J. J., Soetaert, K., & Hagens, M. (2020). Ocean alkalinity, buffering and biogeochemical processes. *Reviews of Geophysics*, *58*(3), e2019RG000681. https://doi.org/10.1029/2019RG000681

Middelburg, J. J., Soetaert, K., & Herman, P. M. J. (1997). Empirical relationships for use in global diagenetic models. *Deep Sea Research Part I: Oceanographic Research Papers*, *44*(2), 327–344. https://doi.org/10.1016/S0967-0637(96)00101-X

Milliman, J. D. (1993). Production and accumulation of calcium carbonate in the ocean: Budget of a nonsteady state. *Global Biogeochemical Cycles*, *7*(4), 927–957. https://doi.org/10.1029/93GB02524

Mitchell, J. S., Mackay, K. A., Neil, H. L., Mackay, E. J., Pallentin, A., & Notman, P. (2012). Undersea New Zealand, 1:5,000,000.

Morse, J. W., Andersson, A. J., & Mackenzie, F. T. (2006). Initial responses of carbonate-rich shelf sediments to rising atmospheric pCO_2 and "ocean acidification": Role of high Mg-calcites. *Geochimica et Cosmochimica Acta*, *70*(23), 5814–5830. https://doi.org/10.1016/j.gca.2006.08.017

Morse, J. W., & Mackenzie, F. T. (1990). *Geochemistry of sedimentary carbonates*. Elsevier.

Müller, G., Börker, J., Sluijs, A., & Middelburg, J. J. (2022). Detrital carbonate minerals in Earth's element cycles. *Global Biogeochemical Cycles*, *36*(5), e2021GB007231. https://doi.org/10.1029/2021GB007231

Müller, J. D., & Gruber, N. (2024). Progression of ocean interior acidification over the industrial era. *Science Advances*, *10*(48), eado3103. https://doi.org/10.1126/sciadv.ado3103

Murdoch, R. C. (1989). The effects of a headland eddy on surface macro-zooplankton assemblages North of Otago Peninsula, New Zealand. *Estuarine, Coastal and Shelf Science*, *29*(4), 361–383. https://doi.org/10.1016/0272-7714(89)90034-6

Najjar, R. G., Herrmann, M., Cintrón Del Valle, S. M., Friedman, J. R., Friedrichs, M. A. M., Harris, L. A., et al. (2020). Alkalinity in tidal tributaries of the Chesapeake Bay. *Journal of Geophysical Research: Oceans*, *125*(1), e2019JC015597. https://doi.org/10.1029/2019JC015597

Otago Regional Council. (2025). Otago Regional Council Environmental data [Dataset]. Retrieved from https://envdata.orc.govt.nz/AQWebPortal

Palmiéri, J., & Yool, A. (2024). Global-Scale evaluation of coastal Ocean alkalinity enhancement in a fully coupled Earth System model. *Earth's Future*, *12*(3), e2023EF004018. https://doi.org/10.1029/2023EF004018

Pinkerton, M., Gall, M., Thoral, F., Sutton, P., & Wood, S. (2024). *Monitoring ocean health: 2023 update on satellite indicators for surface temperature, productivity and suspended solids (monitoring ocean health No. 2023217WN_rev1)*. National Institute of Water and Atmospheric Research Ltd. Retrieved from https://environment.govt.nz/publications/monitoring-ocean-health-2023-update-on-satellite-indicators-for-surface-temperature-productivity-and-suspended-solids/

Precht, E., Franke, U., Polerecky, L., & Huettel, M. (2004). Oxygen dynamics in permeable sediments with wave-driven pore water exchange. *Limnology & Oceanography*, *49*(3), 693–705. https://doi.org/10.4319/lo.2004.49.3.0693

Raymond, P. A., & Cole, J. J. (2001). Gas exchange in rivers and estuaries: Choosing a gas transfer velocity. *Estuaries*, *24*(2), 312–317. https://doi.org/10.2307/1352954

Raymond, P. A., & Cole, J. J. (2003). Increase in the export of alkalinity from North America's largest River. *Science*, *301*(5629), 88–91. https://doi.org/10.1126/science.1083788

R Core Team. (2021). *R: A language and environment for statistical computing*. R Foundation for Statistical Computing. Retrieved from https://www.R-project.org/

Renforth, P., & Henderson, G. (2017). Assessing ocean alkalinity for carbon sequestration. *Reviews of Geophysics*, *55*(3), 636–674. https://doi.org/10.1002/2016RG000533

Ridgwell, A., Hargreaves, J. C., Edwards, N. R., Annan, J. D., Lenton, T. M., Marsh, R., et al. (2007). Marine geochemical data assimilation in an efficient Earth System Model of global biogeochemical cycling. *Biogeosciences*, *4*(1), 87–104. https://doi.org/10.5194/bg-4-87-2007

Ridgwell, A., Zondervan, I., Hargreaves, J. C., Bijma, J., & Lenton, T. M. (2007). Assessing the potential long-term increase of oceanic fossil fuel CO_2 uptake due to CO_2-calcification feedback. *Biogeosciences*, *4*(4), 481–492. https://doi.org/10.5194/bg-4-481-2007

Rusch, A., Huettel, M., Wild, C., & Reimers, C. E. (2006). Benthic oxygen consumption and organic matter turnover in organic-poor, permeable Shelf sands. *Aquatic Geochemistry*, *12*(1), 1–19. https://doi.org/10.1007/s10498-005-0784-x

Santos, I. R., Eyre, B. D., & Huettel, M. (2012). The driving forces of porewater and groundwater flow in permeable coastal sediments: A review. *Estuarine, Coastal and Shelf Science*, *98*, 1–15. https://doi.org/10.1016/j.ecss.2011.10.024

Shears, N. T., & Bowen, M. M. (2017). Half a century of coastal temperature records reveal complex warming trends in western boundary currents. *Scientific Reports*, *7*(1), 14527. https://doi.org/10.1038/s41598-017-14944-2

Smith, A. M., Wood, A. C. L., Liddy, M. F. A., Shears, A. E., & Fraser, C. I. (2010). Human impacts in an urban port: The carbonate budget, Otago Harbour, New Zealand. *Estuarine, Coastal and Shelf Science*, *90*(2), 73–79. https://doi.org/10.1016/j.ecss.2010.07.004

Smith, R. O., Vennell, R., Bostock, H. C., & Williams, M. J. M. (2013). Interaction of the subtropical front with topography around southern New Zealand. *Deep Sea Research Part I: Oceanographic Research Papers*, *76*, 13–26. https://doi.org/10.1016/j.dsr.2013.02.007

Soetaert, K. (2009). rootSolve: Nonlinear root finding, equilibrium and steady-state analysis of ordinary differential equations.

Soetaert, K., Herman, P. M. J., & Middelburg, J. J. (1996). A model of early diagenetic processes from the shelf to abyssal depths. *Geochimica et Cosmochimica Acta*, *60*(6), 1019–1040. https://doi.org/10.1016/0016-7037(96)00013-0

Soetaert, K., & Meysman, F. (2012). Reactive transport in aquatic ecosystems: Rapid model prototyping in the open source software R. *Environmental Modelling and Software*, *32*, 49–60. https://doi.org/10.1016/j.envsoft.2011.08.011

Soetaert, K., Middelburg, J. J., Herman, P. M. J., & Buis, K. (2000). On the coupling of benthic and pelagic biogeochemical models. *Earth-Science Reviews*, *51*(1–4), 173–201. https://doi.org/10.1016/S0012-8252(00)00004-0

Soetaert, K., Petzoldt, T., & Meysman, F. J. R. (2010). Marelac: Tools for Aquatic Sciences R package version 2.1.

Sulpis, O., Agrawal, P., Wolthers, M., Munhoven, G., Walker, M., & Middelburg, J. J. (2022). Aragonite dissolution protects calcite at the seafloor. *Nature Communications*, *13*(1), 1104. https://doi.org/10.1038/s41467-022-28711-z

Sulpis, O., Boudreau, B. P., Mucci, A., Jenkins, C., Trossman, D. S., Arbic, B. K., & Key, R. M. (2018). Current $CaCO_3$ dissolution at the seafloor caused by anthropogenic CO_2. *Proceedings of the National Academy of Sciences*, *115*(46), 11700–11705. https://doi.org/10.1073/pnas.1804250115

Sulpis, O., Humphreys, M. P., Wilhelmus, M. M., Carroll, D., Berelson, W. M., Menemenlis, D., et al. (2022). RADIv1: A non-steady-state early diagenetic model for ocean sediments in Julia and MATLAB/GNU Octave. *Geoscientific Model Development*, *15*(5), 2105–2131. https://doi.org/10.5194/gmd-15-2105-2022

Sutton, A. J., Battisti, R., Carter, B., Evans, W., Newton, J., Alin, S., et al. (2022). Advancing best practices for assessing trends of ocean acidification time series. *Frontiers in Marine Science*, *9*, 1045667. https://doi.org/10.3389/fmars.2022.1045667

Sutton, P. J. H. (2003). The Southland Current: A subantarctic current. *New Zealand Journal of Marine & Freshwater Research*, *37*(3), 645–652. https://doi.org/10.1080/00288330.2003.9517195

van de Velde, S. J. (2025a). Dataset v1.0.0. *Zenodo*. https://doi.org/10.5281/zenodo.17517517

van de Velde, S. J. (2025b). Model code v1.0.0. *Zenodo*. https://doi.org/10.5281/zenodo.17508535

van de Velde, S. J., Hidalgo-Martinez, S., Callebaut, I., Antler, G., James, R. K., Leermakers, M., & Meysman, F. J. R. (2020). Burrowing fauna mediate alternative stable states in the redox cycling of salt marsh sediments. *Geochimica et Cosmochimica Acta*, *276*, 31–49. https://doi.org/10.1016/j.gca.2020.02.021

van de Velde, S. J., Hylén, A., & Meysman, F. J. R. (2025). Ocean alkalinity destruction by anthropogenic seafloor disturbances generates a hidden CO_2 emission. *Science Advances*, *11*(13), eadp9112. https://doi.org/10.1126/sciadv.adp9112

van de Velde, S. J., & Meysman, F. J. R. (2016). The influence of bioturbation on iron and sulphur cycling in marine sediments: A model analysis. *Aquatic Geochemistry*, *22*(5–6), 469–504. https://doi.org/10.1007/s10498-016-9301-7

van de Velde, S. J., Reinhard, C. T., Ridgwell, A., & Meysman, F. J. R. (2020). Bistability in the redox chemistry of sediments and oceans. *Proceedings of the National Academy of Sciences*, *117*(52), 33043–33050. https://doi.org/10.1073/pnas.2008235117

Vance, J. M., Currie, K., Suanda, S. H., & Law, C. S. (2024). Drivers of seasonal to decadal mixed layer carbon cycle variability in subantarctic water in the Munida Time Series. *Frontiers in Marine Science*, *11*, 1309560. https://doi.org/10.3389/fmars.2024.1309560

Vervoort, P., Adloff, M., Greene, S. E., & Kirtland Turner, S. (2019). Negative carbon isotope excursions: An interpretive framework. *Environmental Research Letters*, *14*(8), 085014. https://doi.org/10.1088/1748-9326/ab3318

Volk, T., & Hoffert, M. I. (1985). Ocean carbon pumps: Analysis of relative strengths and efficiencies in ocean-driven atmospheric CO2 changes. In *The carbon cycle and atmospheric CO2: Natural variations Archean to present* (pp. 99–110). American Geophysical Union (AGU). https://doi.org/10.1029/GM032p0099

Zeebe, R. E. (2012). History of seawater Carbonate Chemistry, atmospheric CO2, and Ocean acidification. *Annual Review of Earth and Planetary Sciences*, *40*(1), 141–165. https://doi.org/10.1146/annurev-earth-042711-105521

Zeebe, R. E., & Wolf-Gladrow, D. (2001). *CO2 in seawater: Equilibrium, kinetics, isotopes*. Gulf Professional Publishing.